FRACTAL MEASUREMENT IN THE SPECTRAL DOMAIN

Jaber Rahma, Richard Noël, Fernandez-Maloigne Christine

University of Poitiers, XLIM Laboratory

ABSTRACT

In order to calibrate texture features in the spectral domain, fractal measurement methods are required. This work is dedicated to Hurst exponent measurement in color, multi and hyperspectral domains, as it is directly linked to fractal dimension measurement. Two approaches from the same family are compared, the multivariate box-counting-based approach and the direct assessment from Kolmogorov's expression that we propose. The experiments were done using a generated spectral fractal image dataset and a real hyperspectral image dataset raising questions about the interest of preserving the initial spectral resolution.

***Index Terms*—** spectral imaging, fractal dimension, complexity

1. INTRODUCTION

In order to calibrate texture features in the spectral domain, fractal measurement methods are required [1] (reference production and validation procedure). Since Mandelbrot [2] and the box counting approach [3], several measurement procedures have been proposed including the Probabilistic Box Counting (PBC) [4] or the Differential Box Counting (DBC) [5]. Authors expressed the limitations of box-counting based approaches [6], while also proving that no method is best in terms of all parameters [7].

However, the aforementioned methods were defined for grayscale images and their extension to multivariate cases (color, spectral, multimodal ...) is not straightforward. In [8], an extension of the probabilistic box counting from grayscale to RGB color space was defined considering a 5-dimensional heterogeneous space (x, y, R, G, B). Later, the same author extended the approach to the multispectral domain [9]. In parallel, Nayak et al. adapted the DBC to color images [10]. All these approaches use marginal processing i.e., they consider the color axes as orthogonal, which is never the case (the dot product between the spectral sensitivity functions of any RGB space is never null). In this work, we present a direct method for processing the Hurst exponent of multivariate images, thus determining their fractal dimension. We also compare the obtained results to adapted differential and probabilistic box counting in color, multispectral and hyperspectral domain.

In the following, we shortly describe the box counting with some of its derived approaches and their extension to the multivariate context. Then, we define our proposition consisting of a direct assessment of the Hurst exponent at the core of the fractal dimension assessment. To compare the approaches, two experiments are presented. The first one compares the assessed Hurst exponents to those used for the generation via multivariate fractal image synthesis. The second experiment compares the Hurst exponent processed from real surfaces acquired using a hyperspectral sensor with that processed from the same surfaces but transposed in color and multispectral domains.

2. COMPLEXITY/FRACTAL DIMENSION ESTIMATION

2.1. Initial approaches for univariate images

The fractal adventure mainly begins with the fractional Brownian motion defined by Kolmogorov [11]. It establishes the relationship between the topological dimension of the signal support E ($E = 2$ for an image), H the Hurst exponent and the fractal dimension D. This relationship is defined in (1) and is adapted for particle movement, so univariate signals:

$$D = E + 1 - H \tag{1}$$

Where H is the Hurst exponent between 0 (higher complexity) and 1.0 (lower complexity = uniform surface).

Derived directly from the measurement theory and from the Minkowski-Bouligand dimension, the box counting approach counts the number of boxes of size ϵ required to cover the 1d-signal or 2d-image I. The measurement space is heterogeneous with 2 spatial dimensions added by one intensity dimension for the grey-level values. One unit change in the spatial dimension is related to one unit change in intensity. By construction, larger is the spatial scale ϵ, lower is the number $N_\epsilon(I)$ of boxes required to cover I. The evolution of $N_\epsilon(I)$ according to ϵ provide the box dimension, so the Hurst coefficient. This evolution is defined by the slope of the curve $log(N_\epsilon(I))$ vs $log(\frac{1}{\epsilon})$ and estimated classically by Ordinary Least Square (OLS) method:

$$dim_{box(S)} = \lim_{\epsilon \to 0} \frac{log(N_\epsilon(I))}{log(\frac{1}{\epsilon})} \tag{2}$$

The DBC [5] offers a quick alternative to the box-counting method for approximating $N_\epsilon(I)$. DBC considers only the maximal and minimal intensity values for each spatial support of size $\epsilon \times \epsilon$. For a given spatial location p and a scale ϵ, the number of boxes considered is given by :

$$N_\epsilon(I) \approx \frac{\max_{q=p-\epsilon//2}^{p+\epsilon//2-1} I(q) - \min_{q=p-\epsilon//2}^{p+\epsilon//2-1} I(q)}{\epsilon} \quad (3)$$

Given that the box dimension, so the Hurst coefficient, is assessed in a log-log plane, the authors proposed working in a dyadic scheme using a sequence of ϵ values following a power law.

Finally, the PBC method [4] is slightly different, it considers the probability $p(m, \epsilon)$ of having m cubes of size ϵ covering the surface I. The number of boxes required to cover the surface is then obtained via:

$$N_\epsilon(I) = \sum_{m=1}^{N} \frac{1}{m} p(m, \epsilon) \propto \epsilon^{-H} \quad (4)$$

where $\sum_{m=1}^{N} p(m, \epsilon) = 1$.

2.2. Extension to multivariate images

The natural extension of box-counting based approaches to multivariate images is mainly done using marginal processing, i.e., considering the color or spectral axes as being independent and normed. So the previous expressions are directly transposed in n-dimensional heterogeneous space with 2 spatial axes and m-axes for the multivariate content (e.g., three axes for color) [8, 12]. In [12], the authors consider separately the three color channels before averaging the box count. However in [8], the authors consider for the box size in the color domain the Minkwoski infinity norm rather than a Euclidean distance.

In [13], a straightforward approach based on the fBm expression in the color domain (5) is proposed.

$$E\left[d\Big(I(p) - I(p+\epsilon) \Big)^2 \right] \propto |\epsilon|^{2H} \quad (5)$$

As the subtraction operator is not available in the color and spectral space, the multivariate subtraction between $I(p) - I(q)$ is replaced by a multivariate distance to select according to the application domain. For the color domain, the CIEDE difference applied in CIELAB color space is recommended [13]. In such case, the color difference is correlated to the human's ability to order color pairs according to their color differences. For the spectral domain, the $L2$ metric can be used to stay close to the Kolmogorov expression, or a metrological solution as KLPD can be used.

To improve the assessment accuracy of $E(d(I(y) - I(x))^2)$ in the color domain, the average distance assessment is replaced by the assessment of the three dimensional volume of the color differences $d(I(y) - I(x))$ (6). This volume is proportional to $\sigma_1 \cdot \sigma_2 \cdot \sigma_3$, where σ_i corresponds to the standard-deviation along the principal component axis i, obtained after applying Principal Component Analysis (PCA). The PCA is used to extract the main axes of the ellipsoid formed by the multivariate Gaussian law of $(I(y) - I(x))$. According to the color or spectral content, the difference ellipsoid is not obligatory oriented on the color space axes (L^*, a^* or b^* in CIELAB). The average difference is then approximated by the cubic square root of the volume:

$$E\left(\big(I(p) - I(p+\epsilon) \big)^2 \right) \propto \left(\sqrt[3]{\sigma_1 \cdot \sigma_2 \cdot \sigma_3} \right)^2 \quad (6)$$

$$(\sigma_1 \cdot \sigma_2 \cdot \sigma_3)^{\frac{2}{3}} \propto \|\epsilon\|^{2H} \quad (7)$$

In the following, the extension to the multivariate case, referred to as "spectral fBm" (sfBm), is a straightforward construction from the expression (6). The Hurst coefficient H is given by:

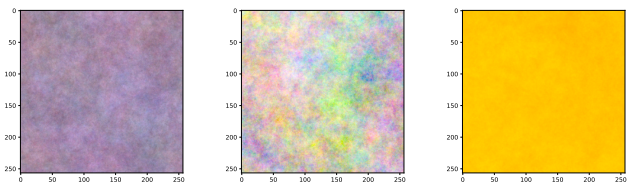
$$E\left(d\big(I(p) - I(p+\epsilon) \big)^2 \right) \propto \left(\prod_{k=1}^{m} \sigma_k \right)^{\frac{2}{n}} \quad (8)$$

with m the band count of the spectra.

For demonstration purposes, we will use our proposed method along with marginal DBC and extended Voss's probabilistic method (Hyperbox) as we can extend both to the spectral domain (n-channels).

3. GENERATED DATA-SET FOR VALIDATION

For the validation of the fractal dimension assessment, fractals are generated in color, multispectral and hyperspectral domains. In each domain, ten fractal images are generated, with Hurst coefficients equal to $H = [0.01, 0.1, 0.2, \ldots, 0.9]$. The color images are generated in CIELAB, to be associated with a valid color difference. The multispectral images are generated considering the spectral bands centered around $\lambda = [400, 450, 500, 550, 600, 650, 700]$nm and an $FWHM \approx 50$ nm. These choices are intended to match the SILIOS CMS-4C multispectral sensor characteristics. The hyperspectral images are generated considering 300-bands in the visible



(a) 3-banded fractal image (b) 7-banded fractal image (c) 300-banded fractal image

Fig. 1. Spectral fractal images with H=0.1 and different color average.

range ($[380, 780]$nm). For the multispectral and hyperspectral cases, the variance-covariance matrix for the fractal generation is an identity matrix multiplied by a factor of 0.0015. Figure 1 shows an example of reconstructed images in RGB using a spectral integration approach aligning with the human visual system (same random seed for the random generation to illustrate the figure differences).

4. ACQUIRED HYPERSPECTRAL DATA-SET

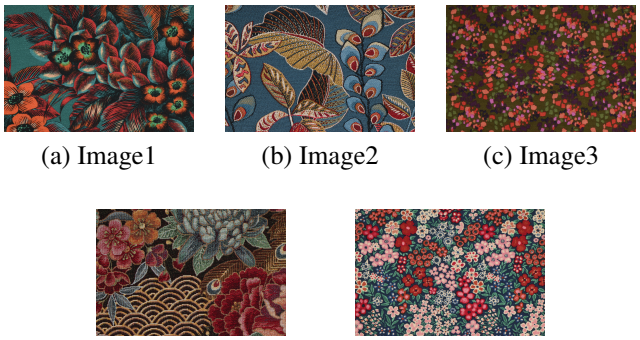
In the context of the SceaLED project, we assess the complexity changes induced on fabrics by changes in light spectra. Figure 2 illustrates five fabrics used in the experiment, a subset of the ten in the full dataset. The images were acquired using the hyperspectral sensor HINALEA 4200 Widefield located at 1 meter from the fabric. The acquisitions were restricted to the range ($[400, 998]$ nm) on 300 bands for an image with 1936×1216 pixels.

As it can be observed, the spatial frequency distribution of the image content is large, with images concentrated on high spatial frequencies (images 3 and 5); Images 1,2 and 4 are showing larger spatial frequencies. For all, the higher spatial frequencies are related to the fabric weave. None of these images correspond to a pure fractal, nevertheless the human visual system is sensitive to a global appearance change due to change in light spectra. We seek to assess this change as a complexity change.

5. RESULTS AND DISCUSSIONS

5.1. Validation on generated hyperspectral images

The multivariate assessment of the Hurst coefficient is done in the generation domain: three channels in the color domain (CIELAB), seven channels in the multispectral domain and three hundred channels in the hyperspectral domain. For the three domains, we estimated the Hurst exponent from the marginal Differential Box Counting (DBC) method expressed by (3), from the marginal probabilistic Box counting (Hyperbox approach expressed by (4)) and from our proposition considering the whole spectra (sfBm approach expressed by (5) for multi and hyperspectral case). The assessment of H is also developed in the trichromatic CIELAB domain using the sfBm approach ($L^*a^*b^*$ measures). For the multispectral and hyperspectral case, the CIELAB images are processed from the generated images in multi or hyperspectral domain according to the CIE recommendations. It is to note that DBC and hyperbox are marginal approaches, by opposition to sfBm that is a vectorial approach.



(a) Image1 (b) Image2 (c) Image3

(d) Image4 (e) Image5

Fig. 2. Real scenes used in application context.

Hurst exponents are estimated from the slope of the log-log plot using Ordinary Least Squares (OLS) method and are presented in table 1. The estimation for the color and multispectral approaches are for ϵ spatial scales from 5 to 100 in steps of 2. For the hyperspectral case, due to the processing cost, the spatial scale ϵ varies between 5 and 80 in steps of 5. Due to problems in the processing of DBC and Hyperbox approaches, the spatial scales are limited to a range varying from 25 to 80 in steps of 5. All the used spatial scales are considered for the estimation, as they theoretically respect the equation (5).

A linear relationship is expected between the generated and the assessed Hurst exponent. To assess the quality of the Hurst exponent measurement, an R^2 coefficient for the linear regression between the generated and the assessed H exponent is provided in the table. The closer the R^2 is to 1.0, the better the assessment will be.

Results from table 1 show that the proposed spectral fBm approach always gets very good regression scores which validates it for spectral images. We also observe that the maximal values obtained by the sfBm decrease with the channel count. Such behavior is induced by the expression (8). When the generated H goes up, the generated complexity decreases and the generated images tend to be flat surfaces. Thus, fewer PCA axes are sufficient to explain the variability. Consequently when the generated H grows, the number of axes with a standard deviation tending to 0 increases, explaining why the slope of the curve H-measured vs H-generated decreases with the channel count. To conclude with this first experiment, the sfBm approach in $L^*a^*b^*$, multi and hyperspectral domains obtains the best regression scores and is valid as a generic fractal measure no matter the application domain.

Despite the marginal nature of the DBC approach, it also shows good regression scores. This result is explained by the selected parameters for the fractal generation. As the variance-covariance matrix used for the generation is based on an identity matrix, the channels are not correlated and a marginal approach can be adapted. In future works, we will explore different spectral constructions considering a complete variance-covariance matrix.

As for the hyperbox approach, as explained by the authors, it is highly sensitive to the range of the spatial scale ϵ. In our experiment, we applied it as a measurement tool with no prior knowledge about the expected result. This explains

Table 1. Hurst exponent assessed from generated color, multi-spectral and hyper-spectral images with specified H.

Generated H	H Color (CIELAB)			H Multi-spectral (7 bands)				H Hyper-spectral (300 bands)			
	Lab	DBC	Hyperbox	Lab	DBC	Hyperbox	sfBm	Lab	DBC	Hyperbox	sfBm
H=0.01	0.097	0.191	0.934	0.078	0.050	0.808	0.082	0.057	-0.046	1.006	0.051
H=0.1	0.136	0.245	1.003	0.111	0.140	0.724	0.117	0.079	0.066	1.000	0.062
H=0.2	0.191	0.249	1.031	0.155	0.267	0.735	0.163	0.109	0.207	1.000	0.076
H=0.3	0.254	0.292	1.034	0.209	0.342	0.809	0.217	0.146	0.283	0.986	0.089
H=0.4	0.323	0.332	1.034	0.269	0.413	0.893	0.276	0.189	0.345	0.993	0.103
H=0.5	0.393	0.404	1.034	0.335	0.463	0.961	0.338	0.236	0.420	0.993	0.115
H=0.6	0.462	0.481	1.034	0.402	0.552	0.999	0.400	0.287	0.486	0.999	0.125
H=0.7	0.526	0.527	1.034	0.470	0.605	1.011	0.459	0.339	0.551	0.999	0.134
H=0.8	0.584	0.596	1.034	0.534	0.657	1.014	0.515	0.389	0.614	0.999	0.142
H=0.9	0.635	0.664	1.034	0.594	0.702	1.014	0.565	0.434	0.663	1.000	0.148
R^2	**0.998**	0.976	0.415	**0.994**	0.980	0.837	**0.998**	**0.991**	0.977	0.007	**0.987**

the reduced regression scores obtained by this approach.

Finally, note that in this experiment, measurement and generation share the same domain. The experiment cannot conclude what number of channels is sufficient for the Hurst exponent measurement of hyperspectral images. And, the high regression scores of the $L^*a^*b^*$ case can be explained by the transposition from the spectral domain to the color domain, done using the CIE recommendations.

5.2. Validation on acquired hyperspectral images

For the second experiment, we compute the Hurst coefficients from hyperspectral images of fabrics. To avoid perturbing the H measure range by an important number of PCA axes without meaningful σ_i (standard-deviation), we retain 90% of the explained variance for the processing of the equation (8). The table 2 presents the obtained results. The fourth image is found to be the most complex, which can be justified by the different textures with various details composing it. Image 5 shows the lowest complexity, followed by images 1, 2 and 3.

	I1	I2	I3	I4	I5
H	0.459	0.409	0.402	0.158	0.626

Table 2. Hurst exponent computed from the hyperspectral images of fabrics (Fig. 2).

6. CONCLUSION

In this work, we introduced and validated the spectral fractional Brownian motion measurement. The approach is directly deduced from Kolmogorov's expression and extended to the spectral domain. Some adjustments remain to be made in order to correct the H measure when the channel count increases. Nevertheless, the proposed measure is linear no matter the channel count, which offers a better solution for complexity assessment using the fractal dimension.

The application on real images is a more complex question. The used fabrics do not correspond to theoretical fractals, consequently, the evolution of the volume facing the spatial scales is far from being linear in the log-log space.

Finally, we require fractal measurement and generation in order to calibrate spectral texture features. As in texture metrology, validating textural attributes needs references and references need to be validated first. We want to have a reference based texture metrology that can be used with multivariate images.

Thanks to this work, we validate fractal measurement and generation, solving a crucial step in our scientific direction.

7. ACKNOWLEDGEMENT

This research was funded, in whole or in part, by the French National Research Agency (ANR) as part of the project SceaLED'ANR-23-CE54-0013-05'

8. REFERENCES

[1] Anne Humeau-Heurtier, "Texture feature extraction methods: A survey," *IEEE Access*, vol. 7, pp. 8975–9000, 2019.

[2] Benoit B. Mandelbrot, *The Fractal Geometry of Nature*, W. H. Freeman and Company, New York, 3rd edition, 1983.

[3] Nirupam Sarkar and Bidyut Baran Chaudhuri, "An efficient approach to estimate fractal dimension of textural images," *Pattern recognition*, vol. 25, no. 9, pp. 1035–1041, 1992.

[4] Richard F Voss, "Random fractals: characterization and measurement," in *Scaling phenomena in disordered systems*, pp. 1–11. Springer, 1986.

[5] N. Sarkar and B.B. Chaudhuri, "An efficient differential box-counting approach to compute fractal dimension of image," *IEEE Transactions on Systems, Man, and Cybernetics*, vol. 24, no. 1, pp. 115–120, 1994.

[6] Jian Li, Qian Du, and Caixin Sun, "An improved box-counting method for image fractal dimension estimation," *Pattern recognition*, vol. 42, no. 11, pp. 2460–2469, 2009.

[7] Chinmaya Panigrahy, Ayan Seal, Nihar Kumar Mahato, and Debotosh Bhattacharjee, "Differential box counting methods for estimating fractal dimension of gray-scale images: A survey," *Chaos, Solitons & Fractals*, vol. 126, pp. 178–202, 2019.

[8] Ivanovici Mihai and Noël Richard, "Fractal dimension of color fractal images," *IEEE Transactions on Image Processing*, vol. 20, no. 1, pp. 227–235, 2010.

[9] Mihai Ivanovici, "A multi-spectral fractal image model and its associated fractal dimension estimator," *Fractal and Fractional*, vol. 7, no. 3, pp. 238, 2023.

[10] Soumya Ranjan Nayak, Jibitesh Mishra, Asimananda Khandual, and Gopinath Palai, "Fractal dimension of rgb color images," *Optik*, vol. 162, pp. 196–205, 2018.

[11] A. N. Kolmogorov, "Wienersche spiralen und einige andere interessante kurven im hilbertschen raum," *C. R. (Doklady) Acad. Sci. URSS (N.S.)*, vol. 26, pp. 115–118, 1940.

[12] Soumya Ranjan Nayak, Abadhan Ranganath, and Jibitesh Mishra, "Analysing fractal dimension of color images," in *2015 International Conference on Computational Intelligence and Networks*, 2015, pp. 156–159.

[13] N Richard, M Ivanovici, and A Bony, "Toward a metrology for non-uniform surface using the complexity notion," in *4th CIE Expert Symposium on Colour and Visual Appearance, Czech Republic, Prague*, 2016, pp. 40–50.